International Journal of
Automotive Manufacturing and Materials (IJAMM)

Scilight

Article

Check for updates

Influence of Suspension Stiffness and Vehicle Speed on Passenger Vehicle Ride Comfort over Random Road Profiles

Anh Nguyen Hoang *, Dien Nguyen Qui, and Dat Pham Le Xuan

Faculty of Automotive Engineering Technology, College of Engineering and Technology (CET), Nam Can Tho University (DNC), 168, Nguyen Van Cu Ext Street, An Binh Ward, Can Tho City 94000, Vietnam
* Correspondence: nhanh@nctu.edu.vn
Received: 16 July 2026; Revised: 17 September 2026; Accepted: 23 October 2026; 3 November 2026

Abstract: Ride comfort is crucial to passenger vehicle design because it affects occupant comfort, stability, and suspension performance. We developed a 7-DOF (seven-degree-of-freedom) spatial full-vehicle dynamic model in MATLAB/Simulink to investigate a passenger car's vibration response to ISO 8608:2016-classified random road profiles. The spatial model represents coupling effects among the four suspension corners by accounting for vehicle-body bounce, pitch, and roll motions, as well as the vertical motion of the unsprung masses, unlike quarter-car and half-car models. The model is compared with simplified vehicle vibration models, and its capabilities are discussed in relation to recent full-vehicle models reported in the literature. The vehicle response is evaluated for road classes B–E, vehicle speeds ranging from 20 to 80 km/h, and suspension stiffness values ranging from 0.5 to 1.5 times the nominal stiffness. Ride comfort is evaluated using Root mean square (RMS), body displacement and vertical acceleration based on ISO 2631-1. Results reveal that road roughness affects vibration response more than vehicle speed. Raising suspension stiffness from 0.5 K to 1.5 K at 80 km/h on a class E road decreases RMS body displacement by 32.8%, while increasing RMS vertical acceleration by 43.8% (from 0.680 to 0.978 m/s^2). These results show the inevitable trade-off between vibration isolation and body-motion inhibition. Because it captures coupled bounce, pitch, and roll responses, the 7-DOF spatial model represents vehicle-body vibration more accurately than vertical-only models, making it better suited for suspension parameter assessment under different road and speed conditions.

Keywords: passenger vehicle; ride comfort; suspension stiffness; vehicle vibration; ISO 8608:2016

1. Introduction

Automobiles play an important role in modern transportation and economic activities and are widely used across various sectors of the economy. With the rapid development of science and technology, the automotive industry worldwide, and in Vietnam in particular, has advanced to meet increasingly high demands, producing a wide range of modern automobiles to serve diverse transportation needs. In vehicle vibration research, road surface irregularities are considered one of the primary sources of vehicle vibration and can induce vertical, longitudinal, and lateral dynamic responses. Many recent studies have adopted the ISO 8608:2016 standard to characterize and simulate stochastic road surface profiles using Power spectral density (PSD) representations [1,2]. Many recent studies have adopted the ISO 8608 standard to characterize and simulate stochastic road surface profiles using power spectral density (PSD) representations [1,2]. Mieteń et al. [3] investigated the dynamic loads acting on a vehicle caused by different road surface profiles and showed that road conditions have a significant influence on the vehicle dynamic response. Wang et al. [4] analyzed the dynamic response of a vehicle–pavement-coupled system based on full-size accelerated loading tests. Xie et al. [5] investigated the dynamic load analysis of vertical, pitching, and lateral tilt vibrations of multi-axle vehicles. Zhao et al. [6] studied road surface classification for vehicle driving assistance.

For passenger cars, which operate under a wide range of road conditions, simulating vehicle vibrations using ISO 8608 road classes is practically important for selecting appropriate operating speeds and evaluating ride comfort. Douier et al. [7] investigated the reconstruction of road roughness profiles using artificial neural networks and dynamic vehicle accelerations. Xing et al. [8] studied road roughness recognition based on feature extraction

Copyright: © 2026 by the authors. This is an open access article under the terms and conditions of the Creative Commons Attribution (CC BY) license (https://creativecommons.org/licenses/by/4.0/).
Publisher's Note: Scilight stays neutral with regard to jurisdictional claims in published maps and institutional affiliations.

and speed-adaptive classification using simulation and real-vehicle tests. Tan et al. [9] proposed a road classification method using a built-in self-scaling method of Bayesian regression. Stan and Oprea [10] reviewed vibration comfort assessment methods, including models, standards, and numerical approaches.

Ride comfort is a crucial indicator of a car's dynamic quality. This measure reflects the extent of mechanical vibrations that are transmitted from the road surface through the suspension system, tires, and chassis to the vehicle's occupants [11,12]. When a car traverses an uneven road surface, random disturbances in the road generate vertical vibrations (bounce), longitudinal vibrations (pitch), and lateral vibrations (roll) in the vehicle's body. Should the amplitude and frequency of these vibrations exceed permissible thresholds, they can lead to discomfort and fatigue for the occupants, impair the driver's concentration, and increase the dynamic load on the car's components, ultimately shortening the structural lifespan and compromising driving safety [13]. The ISO 2631-1:1997 standard is commonly used to assess ride comfort in automotive vibration studies [11]. According to ISO 2631-1, the commonly used criterion is root mean square (RMS) acceleration. In addition to RMS acceleration, maximum acceleration can be used to assess the instantaneous impact level when the vehicle passes over large road irregularities. This value reflects the suspension system's shock-absorption capacity and directly affects the stability of the vehicle and the dynamic loads acting on its components [14]. Besides acceleration, the vehicle body's vertical displacement is also an important quantity that reflects the suspension system's vibration-isolation performance. Excessive vehicle body displacement will reduce the sense of stability, increase the risk of collision between suspension system components and the vehicle frame, and affect control accuracy. Therefore, suspension design generally seeks to reduce both acceleration and vehicle-body displacement by adjusting suspension stiffness and damping coefficients [13].

Because vehicle vibration is coupled in the vertical, pitch, and roll directions, recent research has transitioned from simplified quarter-car and half-car models to full-vehicle spatial models. Xu et al. [15] developed a 14-DOF full-vehicle suspension model to consider the coupled vehicle dynamic responses. Damavandi et al. [16] used a 14-DOF vehicle model to investigate and optimize a hydraulically interconnected suspension system for handling and ride enhancement. Emami et al. [17] investigated a full-vehicle semi-active suspension system considering the impact of uncertainties. These studies demonstrate that full-vehicle spatial models are better suited to describing the interaction among vehicle-body bounce, pitch, roll, and suspension responses than simplified vertical vibration models. For commercial vehicles, the effects of road excitation on cab vibration and ride comfort have also been investigated under different suspension configurations and control strategies [18,19]. Experimental investigations further indicate that road-induced dynamic loads can be transmitted through the suspension system and chassis and therefore should be considered when evaluating vehicle vibration performance [20].

A recent study on ride-comfort optimization with handling restrictions found that suspension settings should be evaluated based on ride and handling performance rather than on vertical acceleration alone [21]. These findings suggest that full-vehicle spatial modeling is better suited to suspension assessment than simplified models, especially when studying interactions among suspension stiffness, vehicle speed, road roughness, and vehicle-body motion. Much research focuses on active or semi-active suspension control and optimization. In contrast, passive suspension stiffness across a wide range of stochastic road classes and vehicle speeds is simple yet practical. Thus, this study uses a 7-DOF passive full-vehicle spatial model to measure how road roughness, vehicle speed, and suspension stiffness affect body displacement and vertical acceleration. Instead of developing a new suspension controller, the goal is to create a computationally efficient spatial model to capture bounce, pitch, and roll coupling for systematic parametric testing [22].

Ride comfort is a crucial indicator of a car's dynamic quality. This measure reflects the extent of mechanical vibrations that are transmitted from the road surface through the suspension system, tires, and chassis to the vehicle's occupants [23]. When a car traverses an uneven road surface, random disturbances in the road generate vertical vibrations (bounce), longitudinal vibrations (pitch), and lateral vibrations (roll) in the vehicle's body [24]. Should the amplitude and frequency of these vibrations exceed permissible thresholds, they can lead to discomfort and fatigue for the occupants, impair the driver's concentration, and increase the dynamic load on the car's components, ultimately shortening the structural lifespan and compromising driving safety [11]. The ISO 2631-1:1997 standard is most commonly used to assess ride comfort in automotive vibration studies. According to ISO 2631, the most commonly used criterion is root mean square acceleration (RMS acceleration), which is defined by the expression [11]:

$$a_\omega = \sqrt{\frac{1}{T}\int_0^T a_\omega^2(t)dt} \tag{1}$$

The smaller the RMS value, the smoother the ride. According to ISO 2631, when the RMS acceleration is less than about 0.315 m/s^2, passengers feel almost no discomfort; from 0.315 to 0.63 m/s^2, vibrations begin to be felt; from about 0.5 to 1.0 m/s^2, it creates a rather uncomfortable feeling; and when it exceeds 1.6 m/s^2, it causes strong discomfort and is unsuitable for prolonged operation [11].

Besides the RMS indicator, many recent studies also use maximum acceleration to assess the instantaneous impact level when the vehicle passes over large bumps. This value reflects the suspension system's shock-absorption capacity and directly affects the stability of the cargo and the load applied to the vehicle frame structure [14].

Besides acceleration, the vehicle body's vertical displacement is also an important quantity that reflects the suspension system's vibration-isolation performance. Excessive vehicle body displacement will reduce the sense of stability, increase the risk of collision between suspension system components and the vehicle frame, and affect control accuracy. Therefore, suspension design generally seeks to reduce both acceleration and vehicle-body displacement by optimizing suspension stiffness and damping coefficients [14].

In the overall vehicle vibration model, in addition to vertical motion, there are also oscillations in pitch and roll angles. The pitch angle directly affects the feeling of acceleration and braking [5]. In contrast, the roll angle determines stability during cornering and when the two wheels pass over uneven bumps. Many studies have shown that reducing the pitch and roll oscillation amplitude not only improves ride comfort but also enhances traction, reduces dynamic wheel load, and increases vehicle motion stability.

To provide a more balanced interpretation of the conflicting effects of suspension stiffness, a normalized multi-objective performance index is introduced. The index combines RMS vertical acceleration and RMS body displacement:

$$J = \omega_c \frac{a_{RMS}}{a_{RMS,ref}} + \omega_d \frac{x_{RMS}}{x_{RMS,ref}} \tag{2}$$

where ω_c and ω_d are weighting factors satisfying $\omega_c + \omega_d = 1$. The reference values are taken from the baseline suspension configuration. A lower value of J indicates a more favorable compromise between vibration isolation and body-motion control. This formulation follows the principle of multi-objective suspension assessment reported by Damavandi et al. [16], who demonstrated that ride and handling requirements can conflict and therefore should be evaluated simultaneously.

Although the use of a passive full-vehicle model is not new by itself, this study provides a systematic framework for quantifying the combined effects of road roughness, vehicle speed, and suspension stiffness on vehicle-body vibration. Four ISO 8608 road classes (B–E), vehicle speeds of 20–80 km/h, and three suspension stiffness levels (0.5 K, K, and 1.5 K) are investigated using the same seven-degree-of-freedom spatial model. The results reveal the trade-off between vibration isolation and body-motion control, showing that increased suspension stiffness can reduce body displacement while increasing vertical acceleration under severe road excitation. A normalized multi-objective performance index is also introduced for comparative assessment. Therefore, the main contribution is the systematic quantification and comparative assessment of passive suspension stiffness under combined variations in stochastic road roughness and vehicle speed.

The remainder of this paper is organized as follows. Section 2 presents the assumptions, development, and governing equations of the seven-degree-of-freedom full-vehicle vibration model, together with the simulation approach based on ISO 8608:2016 road profiles. Section 3 investigates the effects of suspension stiffness and vehicle speed on vehicle body displacement and vertical acceleration under different road conditions. The simulation results are analyzed using RMS-based ride-comfort indicators to evaluate the trade-off between vibration isolation and body-motion control. Finally, Section 4 summarizes the main findings and presents the key conclusions of the study.

2. Developing a Model to Evaluate the Ride Comfort of Automobiles

2.1. Some Initial Hypotheses

To build the model, the following assumptions are necessary:

The vehicle's mass is distributed symmetrically in the longitudinal plane; when fully loaded with goods and treated as solid mass, the suspended mass is considered absolutely rigid.

Ignoring the effect of wheel slippage, the road surface is considered to have very little deformation.

The tire–road contact is assumed to be a point contact, and the vehicle is assumed to travel in a straight line at a constant speed.

2.2. Building a Model

Figure 1 shows the model that studies the oscillation of a vehicle around its static equilibrium position while it moves on a road.

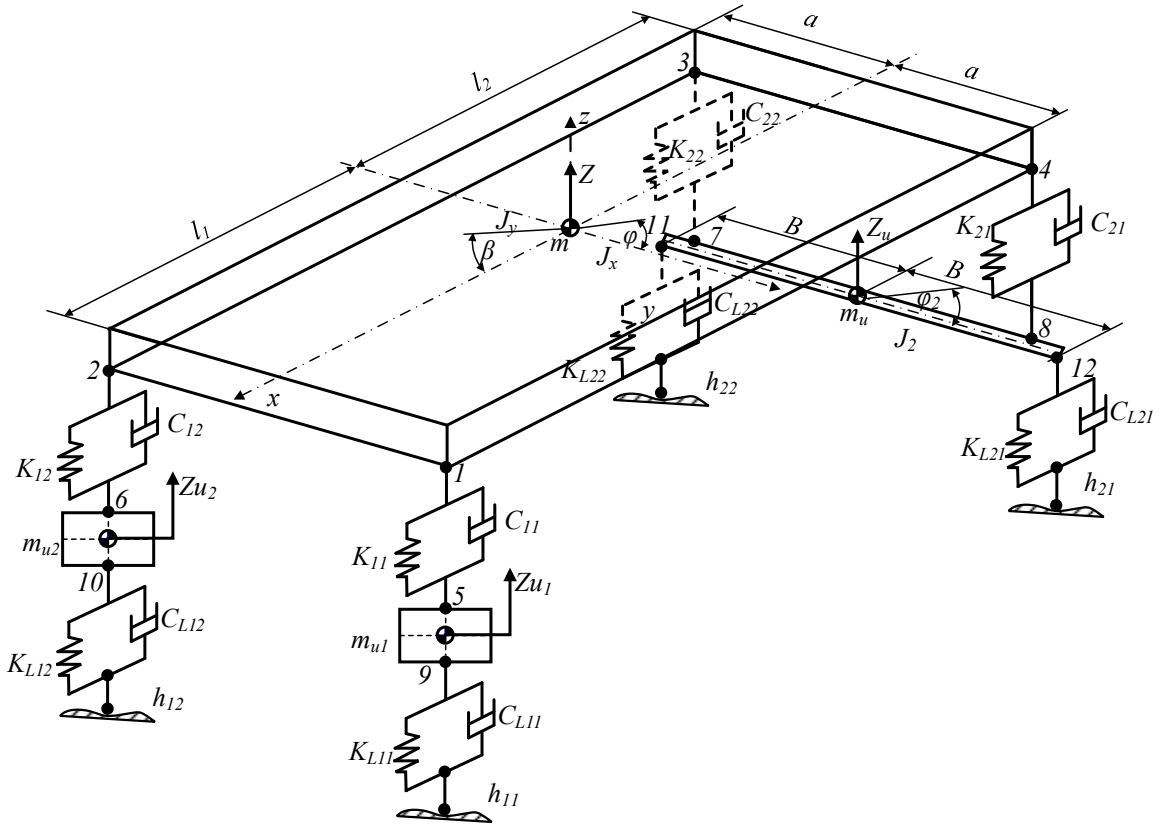


Figure 1. Vehicle oscillation model.

Model Parameters:

+ Z—Vertical displacement of the sprung mass along the z-axis.
+ Z_{u1}, Z_{u2}—Vertical displacements of the left-front and right-front unsprung masses, respectively.
+ m—Sprung mass of the vehicle.
+ m_{u1}, m_{u2}—Unsprung masses of the left-front and right-front wheels, respectively.
+ J_x—Mass moment of inertia of the sprung mass about the x-axis (roll axis).
+ J_y—Mass moment of inertia of the sprung mass about the y-axis (pitch axis).
+ m_u—Unsprung mass of the rear axle.
+ J_2—Mass moment of inertia of the rear unsprung mass about the x-axis.
+ φ—Roll angle of the sprung mass about the x-axis.
+ β—Pitch angle of the sprung mass about the y-axis.
+ φ_2—Roll angle of the rear unsprung mass about the x-axis.
+ K_1, K_2—Suspension stiffnesses of the front, and rear suspensions, respectively.
+ C_1, C_2—Suspension damping coefficients of the front, and rear dampers, respectively.
+ K_{L1}, K_{L2}—Tire stiffnesses of the front, and rear tires, respectively.
+ C_{L1}, C_{L2}—Tire damping coefficients of the front, and rear tires, respectively.
+ B—Half of the vehicle track width.
+ a—Lateral distance from the vehicle centerline to the left or right suspension mounting point.
+ l_1—Longitudinal distance from the vehicle Center of gravity (CG) to the front axle.
+ l_2—Longitudinal distance from the vehicle Center of gravity (CG) to the rear axle.
+ h_{11}, h_{12}, h_{21}, h_{22}—Road surface elevations (road input excitations) at the left-front, right-front, left-rear, and right-rear wheels, respectively.

The main parameters of the vehicle dynamic model used in this study are presented in Table 1.

Table 1. Model 2 parameters.

Order	Name	Symbol	Unit	Value
1	Sprung mass	m	kg	1920
2	Mass moment of inertia of the sprung mass about the x-axis	J_x	kg·m^2	4403
3	Mass moment of inertia of the sprung mass about the y-axis	J_y	kg·m^2	16,645
4	Suspension stiffnesses of the front	K_1	N/m	175,000
5	Suspension stiffnesses of the rear	K_2	N/m	326,000
6	Tire stiffnesses of the front tires	K_{L1}	N/m	350,000
7	Tire stiffnesses of the rear tires	K_{L2}	N/m	652,000
8	Suspension damping coefficients of the front	C_1	N·s/m	6090
9	Suspension damping coefficients of the rear	C_2	N·s/m	7675
10	Tire damping coefficients of the front tires	C_{L1}	N·s/m	7985
11	Tire damping coefficients of the rear tires	C_{L2}	N·s/m	8640
12	Unsprung mass of the rear axle	m_u	kg	300
13	Mass moment of inertia of the rear unspring mass about the x-axis	J_2	kg·m^2	335
14	Lateral distance from the vehicle centerline to the left or right suspension mounting point	a	mm	124
15	Half of the vehicle track width	B	mm	170

2.3. Differential Equations Describing Vehicle Oscillations

Applying Newton-Euler equations to the system's motion, we establish the following system of differential equations for oscillation:

$$\begin{aligned} &m*\ddot{Z}+C_1*\left(2*\dot{Z}+2*\dot{\beta}*l_1-\dot{Z}_{u1}-\dot{Z}_{u2}\right)+K_1*\left(2*Z+2*\beta*l_1-Z_{u1}-Z_{u2}\right)\\ &+C_2*\left(2*\dot{Z}-2*\dot{\beta}*l_2-2*\dot{Z}_u\right)+K_2*\left(2*Z-2*\beta*l_2-2*Z_u\right)=0 \end{aligned} \tag{3}$$

$$\begin{aligned} &\mathrm{J}_x*\ddot{\varphi}+C_1*a*\left(2*\dot{\varphi}*a-\dot{Z}_{u1}+\dot{Z}_{u2}\right)+K_1*a*\left(2*\varphi*a-Z_{u1}+Z_{u2}\right)\\ &+2*C_2*a^2*\left(\dot{\varphi}-\dot{\varphi}_u\right)+2*K_2*a^2*\left(\varphi-\varphi_u\right)=0 \end{aligned} \tag{4}$$

$$\begin{aligned} &\mathrm{J}_y*\ddot{\beta}+C_1*l_1*\left(2*\dot{Z}+2*\dot{\beta}*l_1-\dot{Z}_{u1}-\dot{Z}_{u2}\right)+K_1*l_1*\left(2*Z+2*\beta*l_1-Z_{u1}-Z_{u2}\right)\\ &-2*C_2*l_2*\left(\dot{Z}-\dot{\beta}*l_1-\dot{Z}_u\right)-2*K_2*l_2\left(Z-\beta*l_2-Z_u\right)=0 \end{aligned} \tag{5}$$

$$\begin{aligned} &m_{u1}*\ddot{Z}_{u1}+C_1*\left(\dot{Z}_{u1}-\dot{Z}-\dot{\varphi}*a-\dot{\beta}*l_1\right)+K_1*\left(Z_{u1}-Z-\varphi*a-\beta*l_1\right)\\ &+C_{L1}*\left(\dot{Z}_{u1}-\dot{h}_{11}\right)+K_{L1}*\left(Z_{u1}-h_{11}\right)=0 \end{aligned} \tag{6}$$

$$\begin{aligned} &m_{u2}*\ddot{Z}_{u2}+C_1*\left(\dot{Z}_{u2}-\dot{Z}+\dot{\varphi}*a-\dot{\beta}*l_1\right)+K_1*\left(Z_{u2}-Z+\varphi*a-\beta*l_1\right)\\ &+C_{L1}*\left(\dot{Z}_{u2}-\dot{h}_{12}\right)+K_{L1}*\left(Z_{u2}-h_{12}\right)=0 \end{aligned} \tag{7}$$

$$\begin{aligned} &m_u*\ddot{Z}_u+2*C_2*\left(\dot{Z}_u-\dot{Z}+\dot{\beta}*l_2\right)+2K_2*\left(Z_u-Z+\beta*l_2\right)\\ &+C_{L2}*\left(2*\dot{Z}_u-\dot{h}_{21}-\dot{h}_{22}\right)+K_{L2}*\left(2*Z_u-h_{21}-h_{22}\right)=0 \end{aligned} \tag{8}$$

$$\begin{aligned} &J_u*\ddot{\varphi}_u+2*C_2*a^2\left(\dot{\varphi}_u-\dot{\varphi}\right)+2*K_2*e^2\left(\varphi_u-\varphi\right)\\ &+C_{L2}*B*\left(2*\dot{\varphi}_u*\mathrm{B}-\dot{h}_{21}+\dot{h}_{22}\right)+K_{L2}*B*\left(2*\varphi_u*\mathrm{B}-h_{21}+h_{22}\right)=0 \end{aligned} \tag{9}$$

2.4. Survey of Passenger Vehicle Vibration

Based on the differential equations describing the mechanical system's oscillations, the study used utility libraries in MATLAB's Simulink to simulate the oscillatory model of the vehicle (Figure 2).

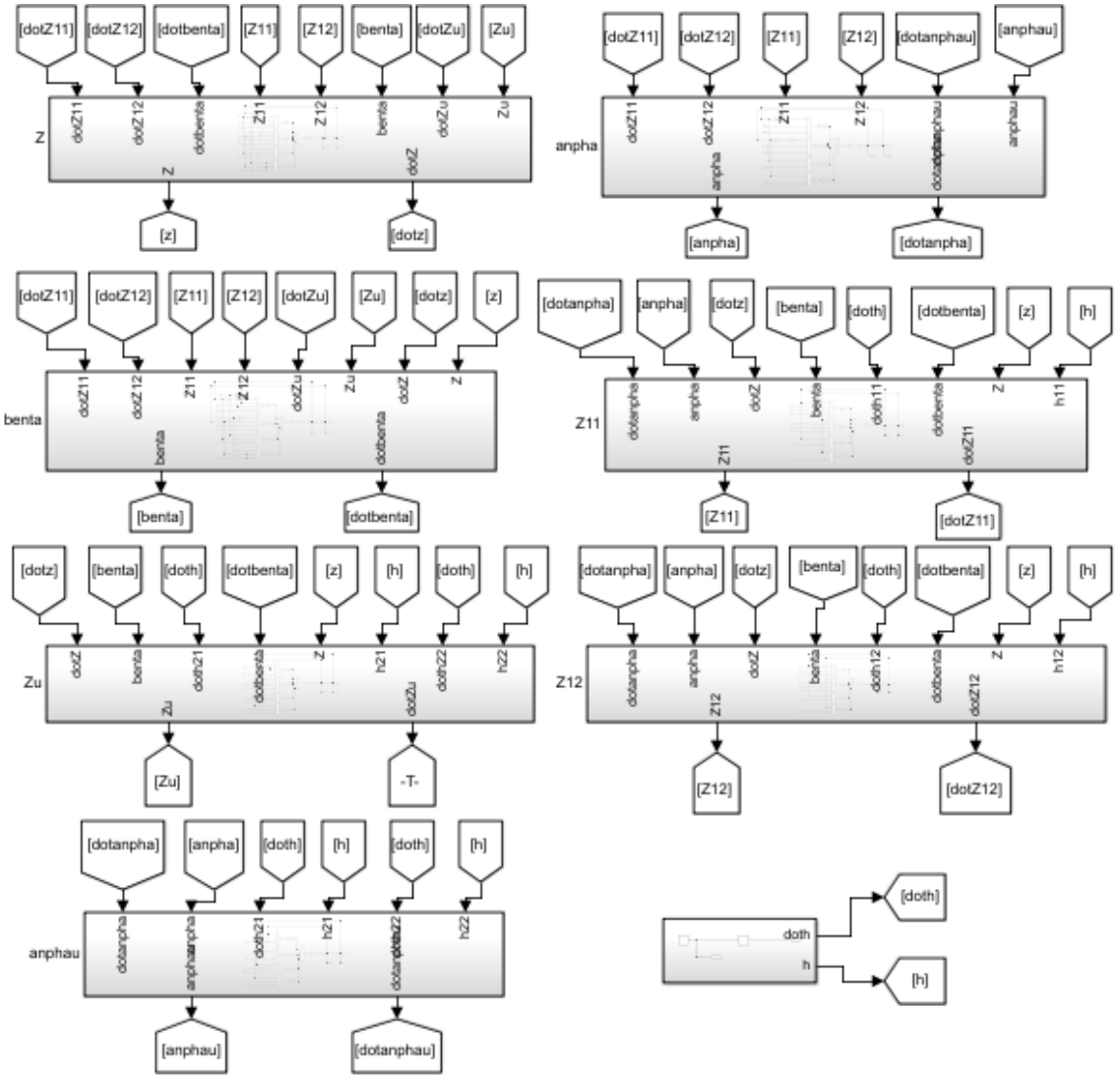


Figure 2. Diagram simulating the vehicle's oscillations.

In this study, simulations were performed for straight-line vehicle motion, with road excitation generated according to ISO 8608:2016. Road surface irregularities defined according to ISO 8608:2016 were used as excitation inputs to investigate the vehicle's dynamic response under representative road conditions. These road-induced excitations generate vehicle-body acceleration, displacement, and roll responses that affect ride comfort. Therefore, surveying vehicle vibrations when driving on standard road surfaces is necessary. The surface irregularities of 7 types of roads, according to ISO 8608:2016, are shown over a 1000 m length, as depicted in Figure 3 [1].

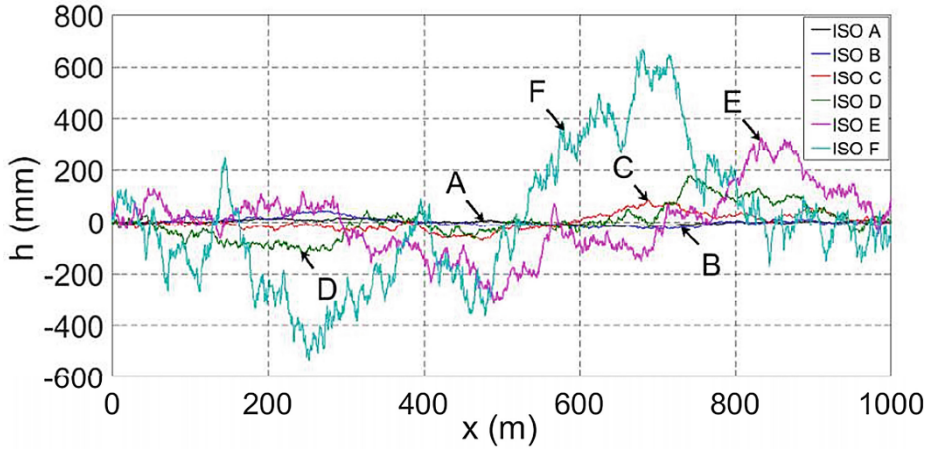


Figure 3. Road surface irregularities according to ISO 8608:2016 standards.

It should be noted that the amplitude of the generated road profile represents the vertical displacement of the road surface and should not be directly compared with the vehicle-body displacement. The road excitation is transmitted through the tires and suspension system, which attenuates and modifies the input excitation before it reaches the sprung mass. Therefore, the body displacement can be substantially smaller than the road-profile amplitude. Nevertheless, the road-profile scaling and amplitude used for each ISO 8608 road class were carefully rechecked to ensure that the generated profiles are physically consistent with the specified road roughness levels.

Figures 4–12 show simulated vehicle body displacement and vertical acceleration for vehicles running on ISO 8608 road classes B, C, D, and E at speeds of 20 to 80 km/h. Generally, both road roughness and vehicle velocity significantly influence the vibration characteristics of the vehicle body.

The class B road (Figures 4 and 5) with a high-quality pavement presents relatively minor body displacement and vertical acceleration. The maximum displacement is still around ±7 mm, and the vertical acceleration is usually below ±0.4 m/s^2. The vibration intensity increases marginally with vehicle speed, while responses remain steady, demonstrating that the suspension system can successfully isolate road-induced excitations under favorable road conditions.

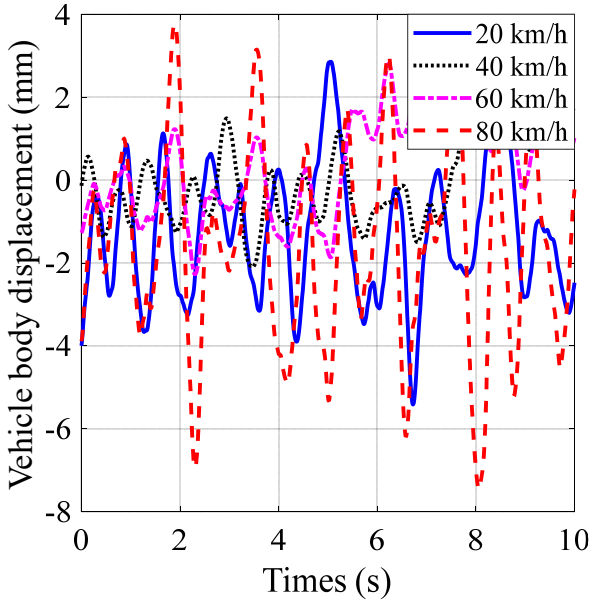


Figure 4. Vehicle body displacement, velocity 20–80 km/h, on class B.

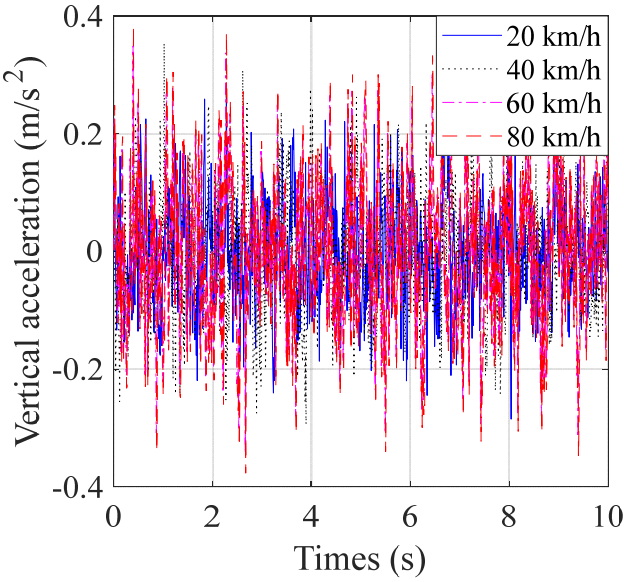


Figure 5. Vertical acceleration of the vehicle body, velocity 20–80 km/h, on class B.

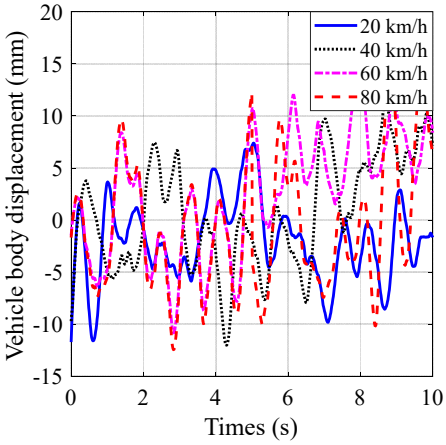


Figure 6. Vehicle body displacement, velocity 20–80 km/h, on class C.

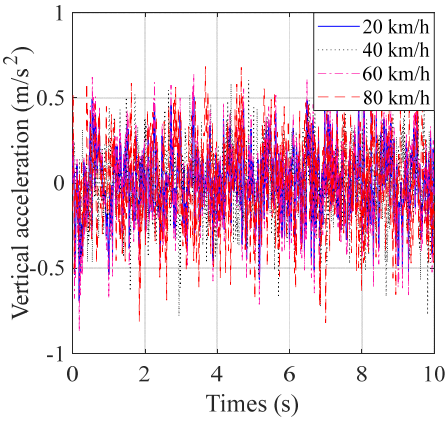


Figure 7. Vertical acceleration of the vehicle body, velocity 20–80 km/h, on class C.

The amplitudes of body displacement and acceleration: Deteriorating Road quality significantly increases the amplitudes of body displacement and acceleration. On class C (Figures 6 and 7) with deteriorating road quality. The max body displacement is roughly ± 15 mm, and the max vertical acceleration is approximately ± 1.0 m/s^2. The increase can be more pronounced at higher vehicle speeds (60–80 km/h), indicating that the combination of a higher excitation frequency and road roughness results in stronger vibration transmission to the vehicle body.

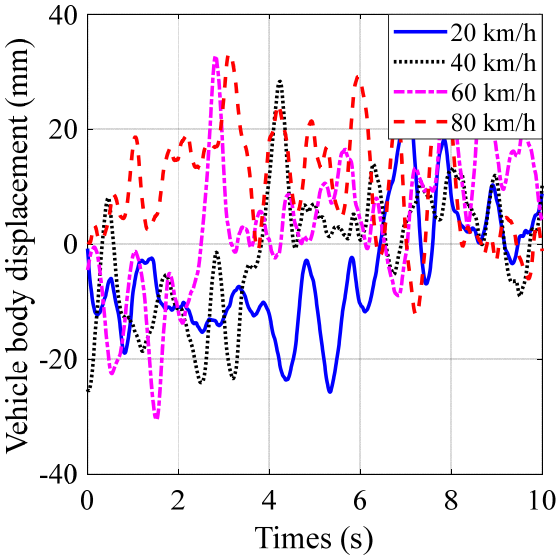


Figure 8. Vehicle body displacement, velocity 20–80 km/h, on class D.

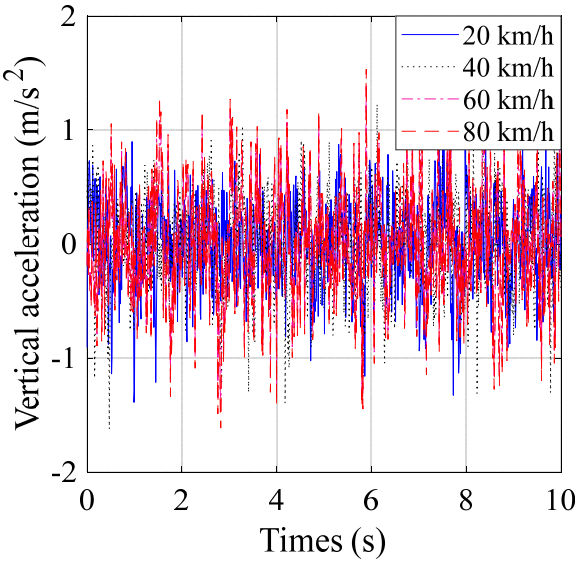


Figure 9. Vertical acceleration of the vehicle body, velocity 20–80 km/h, on class D.

For class D roads (Figures 8 and 9), which correspond to poor road surfaces, the dynamic response increases considerably. The max body displacement is over ±30 mm, and the max vertical acceleration is over ±2.0 m/s^2. When subjected to heavy excitation, the suspension system reaches its performance limits, as evidenced by increasingly erratic vibration signals with larger fluctuations. The responses are further amplified at higher speeds due to increased dynamic loading.

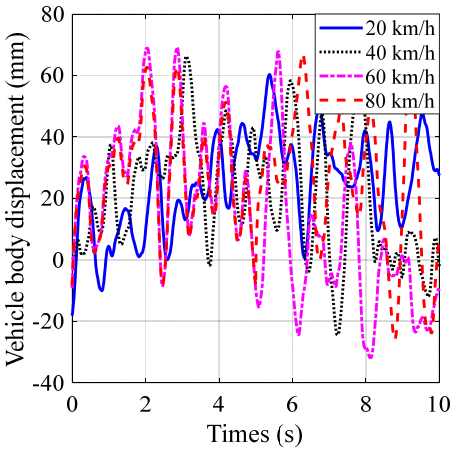


Figure 10. Vehicle body displacement, velocity 20–80 km/h, on class E.

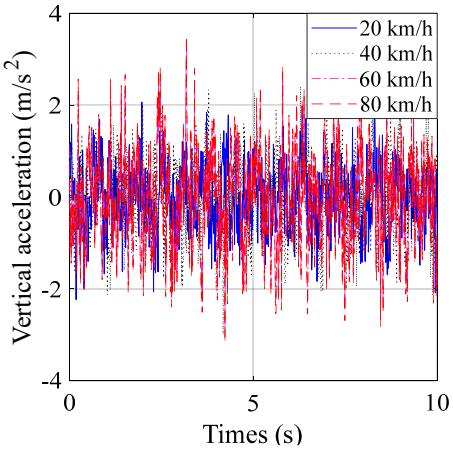


Figure 11. Vertical acceleration of the vehicle body, velocity 20–80 km/h, on class E.

The highest vibration values are obtained for the class E road (Figures 10 and 11), which corresponds to a very poor road state. The max vehicle body displacement is around ±70 mm, and the max vertical acceleration is about ±4.0 m/s^2. The simulation shows large oscillations throughout, especially at 60 km/h and 80 km/h. The results show a considerable reduction in ride comfort and suggest that long-term operation at high speed on these types of roads can negatively impact both passenger comfort and fatigue durability of suspension and chassis components.

The simulation results, in general, show that vehicle vibration increases regularly with increasing road roughness and traveling speed. Of these two parameters, road surface quality has the greatest influence on the vehicle body's displacement and vertical acceleration, and the dynamic response is further amplified as speed increases. The results emphasize the need to select appropriate vehicle speeds for different road conditions and optimize suspension characteristics to enhance ride comfort and reduce structural vibrations. The RMS values of vehicle-body displacement and vertical acceleration under different road conditions and vehicle speeds are summarized in Table 2.

Table 2. RMS vehicle body displacement, RMS vertical body acceleration when the vehicle is moving on the road at different speeds.

Value	Root Mean Square (RMS) Vehicle Body Displacement (mm)				Root Mean Square (RMS) Vertical Body Acceleration (m/s^2)			
Velocity (km/h)	**20**	**40**	**60**	**80**	**20**	**40**	**60**	**80**
On class B	0.90	1.22	1.71	2.37	0.065	0.080	0.092	0.101
On class C	3.40	4.51	5.23	6.13	0.151	0.172	0.190	0.202
On class D	8.74	9.95	10.50	11.43	0.296	0.320	0.350	0.387
On class E	22.86	23.61	25.45	28.70	0.544	0.653	0.754	0.829

As demonstrated in Figure 12, the RMS vehicle body displacement increases constantly with vehicle speed and road roughness. The RMS displacement for the class B road increases from 0.90 mm at a speed of 20 km/h to 2.37 mm at a speed of 80 km/h. For road quality class C and class D, the RMS displacement increases dramatically to 6.13 mm and 11.43 mm at 80 km/h, respectively. The maximum displacement occurs on the class E road, where the RMS value increases from 22.86 mm to 28.70 mm as the vehicle speed increases from 20 to 80 km/h. This trend suggests that body displacement is more affected by road roughness than by vehicle speed, and that higher speed further worsens the vibration response.

The RMS of vertical body acceleration is shown in Figure 13. The RMS acceleration for class B road conditions is quite low, ranging from 0.065 m/s^2 to 0.101 m/s^2, indicating satisfactory ride comfort. But the acceleration always increases on a rougher road surface. At 80 km/h, the RMS accelerations on class C, D, and E roads were 0.202 m/s^2, 0.387 m/s^2, and 0.829 m/s^2, respectively. The increase in vertical acceleration is particularly noticeable in poor road conditions, where larger road irregularities generate higher dynamic excitations that are transmitted to the vehicle body via the suspension system.

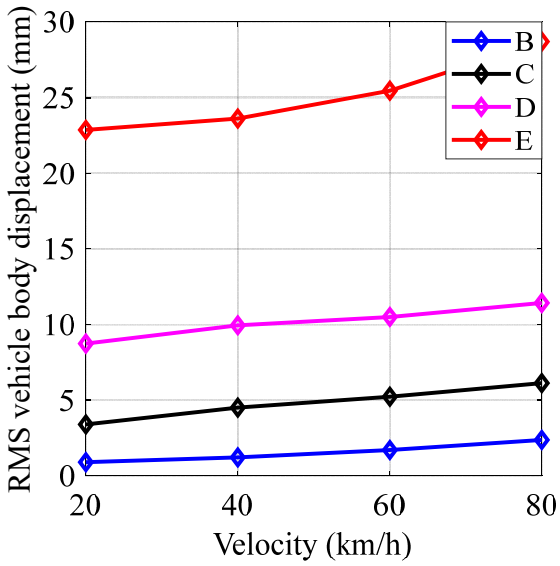


Figure 12. Root mean square vehicle body displacement, v = 20 ÷ 80 km/h.

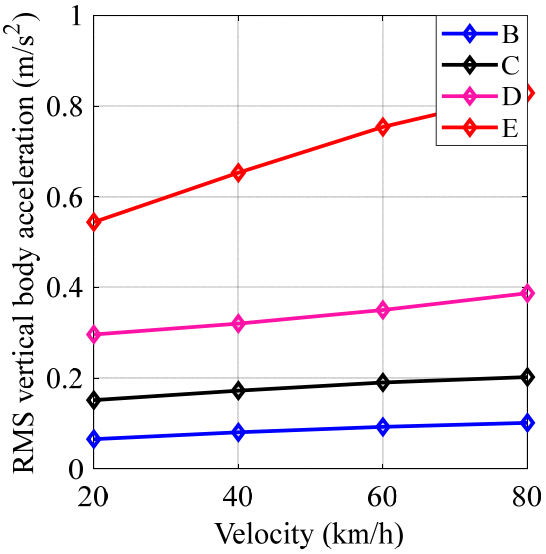


Figure 13. Root mean square vertical body acceleration, v = 20 ÷ 80 km/h.

The results show that speed and road roughness greatly affect vehicle ride performance. The rise in RMS body displacement and vertical acceleration is largely due to poor road conditions. The results show that reducing vehicle speed on uneven roads significantly reduces vehicle vibration, enhancing ride comfort and reducing suspension and chassis dynamic loads.

3. The Effect of Suspension Stiffness on Vehicle Ride Comfort

The stiffness of the elastic element is the characteristic property of a suspension system. This is one of the factors known to influence a car's vibration response significantly. The suspension system's high rigidity transfers road vibrations to the vehicle body, increasing vibration acceleration and reducing ride comfort. However, too low rigidity enhances vibration isolation but tends to increase vehicle body displacement and roll angle, thereby diminishing stability and control, especially at high speed or on uneven roads.

This content analyses the effect of suspension stiffness on ride comfort for vehicles traveling over random road surfaces, based on the ISO 8608:2016 standard. The suspension stiffness values were changed from 0.5 to 1.5 times the baseline values. The findings of the research allow for evaluating the potential to enhance ride comfort and for recommending the appropriate stiffness of passenger cars in real-world operating conditions. Figure 14 illustrates the vehicle-body displacement on a class B road at a speed of 80 km/h for different suspension stiffness values.

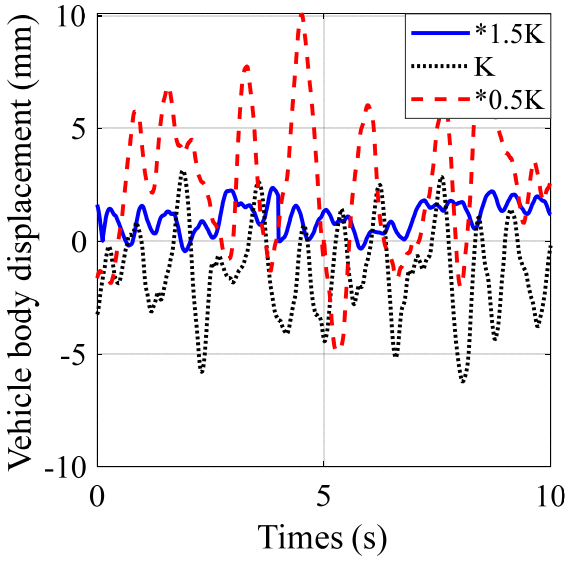


Figure 14. Vehicle body displacement, velocity 80 km/h, on class B when changing stiffness suspension.

On class B roads (Figure 14), the displacement is quite minor for all stiffness values. This is owing to the low road excitation. But the suspension with 1.5 times the original stiffness gives the least body movement, and the suspension with 0.5 times the initial stiffness gives the most body movement. This tendency is especially evident on class C and class D roads (Figures 15 and 16), where increasing suspension stiffness strongly limits body motion and enhances vehicle stability. The most significant difference was observed on road type E (Figure 17). Suspension stiffness at 0.5 times the initial value produced the greatest vehicle body displacement, while stiffness suspension at 1.5 times the initial value effectively limited vehicle body movement under strong road surface impacts.

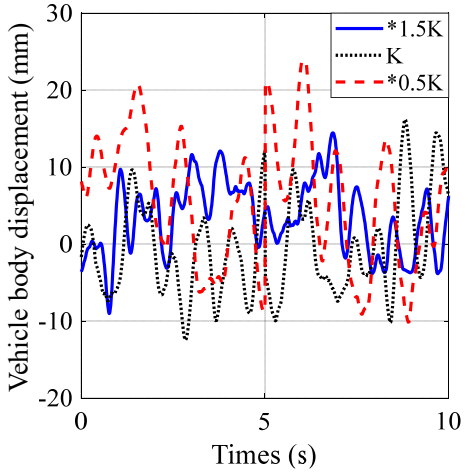


Figure 15. Vehicle body displacement, velocity 80 km/h, on class C when changing stiffness suspension.

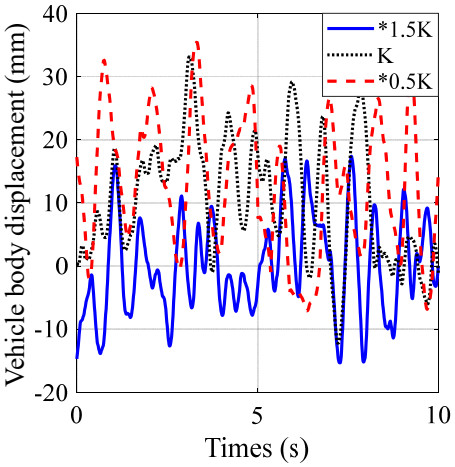


Figure 16. Vehicle body displacement, velocity 80 km/h, on class D when changing stiffness suspension.

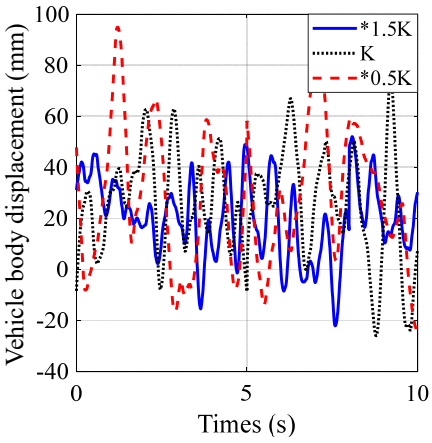


Figure 17. Vehicle body displacement, velocity 80 km/h, on class E when changing stiffness suspension.

On the class B road (Figure 18), the differences among the three stiffness configurations are relatively small because the road excitation is limited. However, on road types C and D (Figures 19 and 20), changing the suspension stiffness by 0.5 to 1.5 times the initial value results in higher acceleration amplitude, although body displacement is reduced. This indicates that a stiffer suspension improves body stability but transmits more vibration energy to the vehicle body.

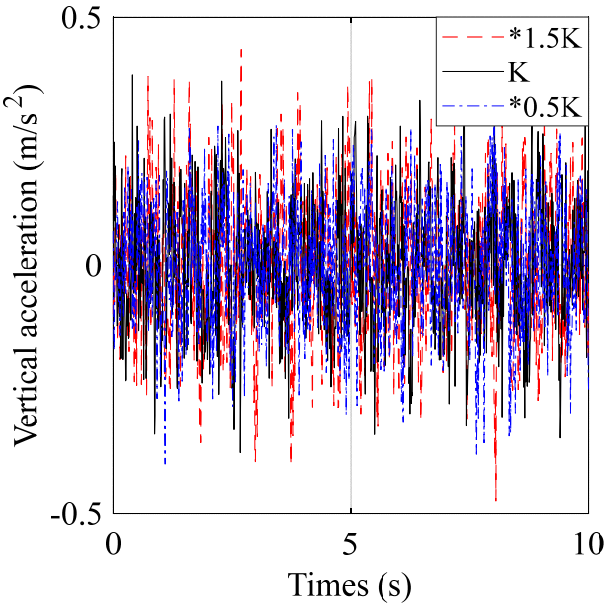


Figure 18. Vertical acceleration of the vehicle body, velocity 80 km/h, on class B when changing suspension stiffness.

The same trend is more pronounced on road type E (Figure 21), where the maximum acceleration occurs with suspension stiffness 1.5 times the initial value, and the minimum acceleration occurs with stiffness suspension 0.5 times the initial value, but the body displacement is larger. These results show a trade-off between driving comfort and control of body movements. Therefore, the choice of the right suspension stiffness is important to achieve a trade-off between reduced body roll and adequate driving comfort across different road conditions.

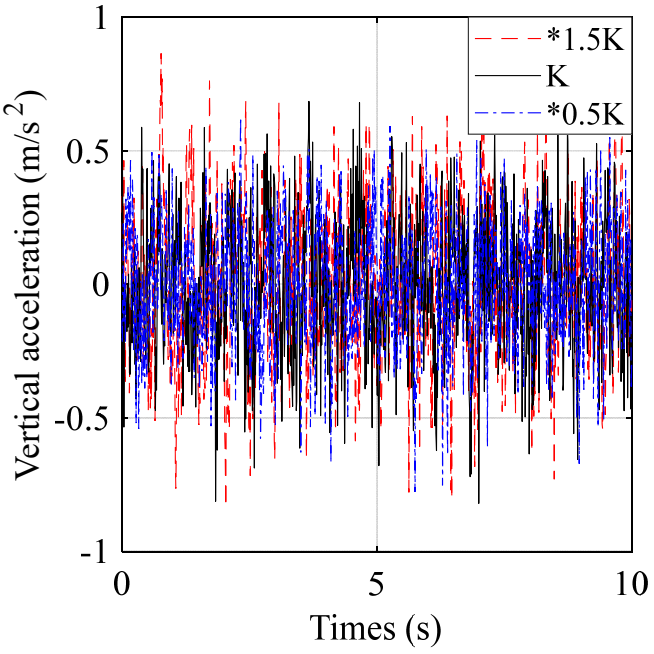


Figure 19. Vertical acceleration of the vehicle body, velocity 80 km/h, on class C when changing stiffness suspension.

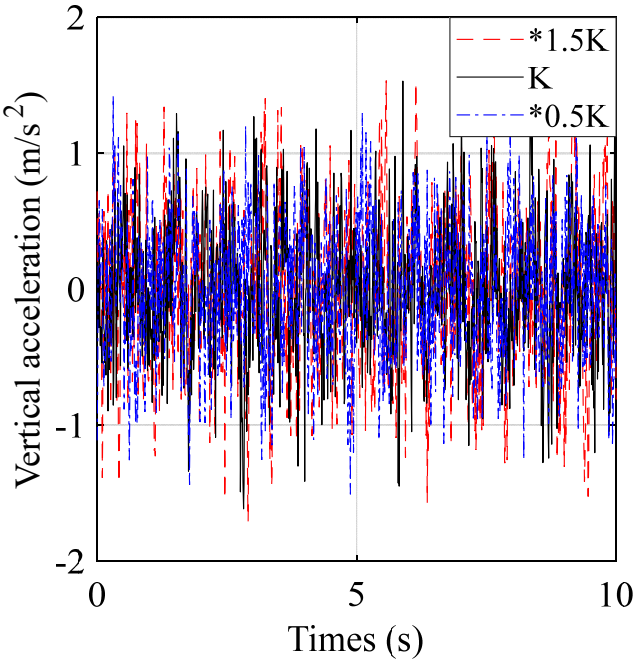


Figure 20. Vertical acceleration of the vehicle body, velocity 80 km/h, on class D when changing stiffness suspension.

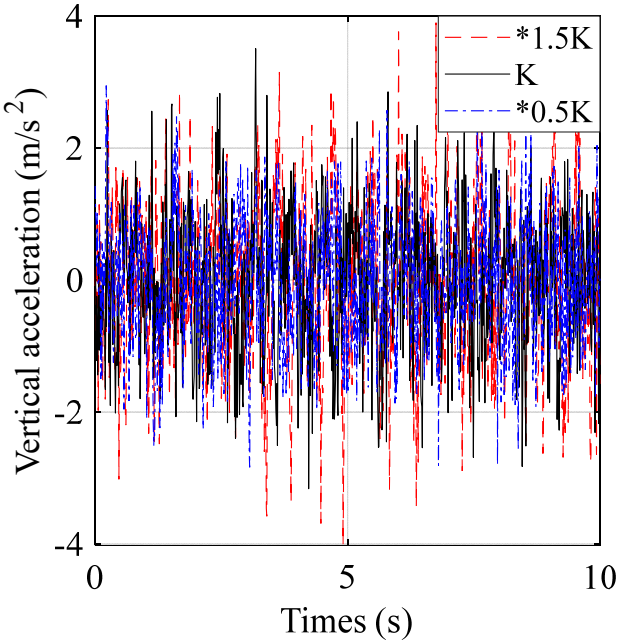


Figure 21. Vertical acceleration of the vehicle body, velocity 80 km/h, on class E when changing stiffness suspension.

To further illustrate the trade-off between body-motion control and vibration isolation, the RMS vehicle-body displacement is plotted against the RMS vertical body acceleration for the investigated suspension stiffness levels and vehicle speeds. The resulting RMS displacement–acceleration relationship provides a complementary representation of the suspension performance that cannot be obtained from either RMS displacement or RMS acceleration alone. As suspension stiffness increases from 0.5 K to 1.5 K, the operating points generally move toward lower RMS displacement but higher RMS acceleration. This confirms the inherent trade-off between reducing vehicle-body motion and limiting vibration transmission to the vehicle body. Figure 22 presents this relationship with class B roads, where the RMS displacement and acceleration remain relatively low. Figure 23 shows the corresponding results for class C roads, with higher vibration levels. Figure 24 illustrates the further increase in both response measures under class D road excitation. Figure 25 extends the comparison to class E roads, where the trade-off becomes more pronounced.

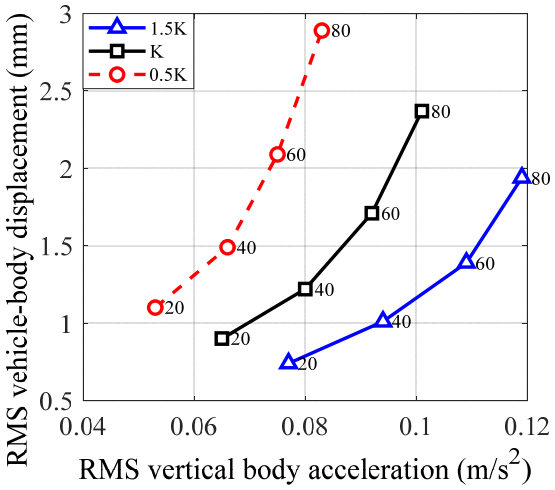


Figure 22. RMS displacement–acceleration trade-off on class B.

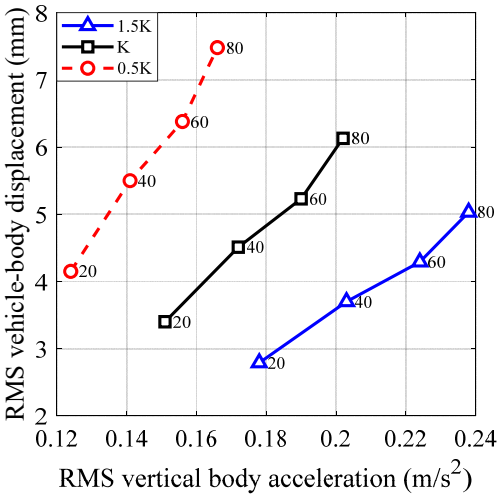


Figure 23. RMS displacement–acceleration trade-off on class C.

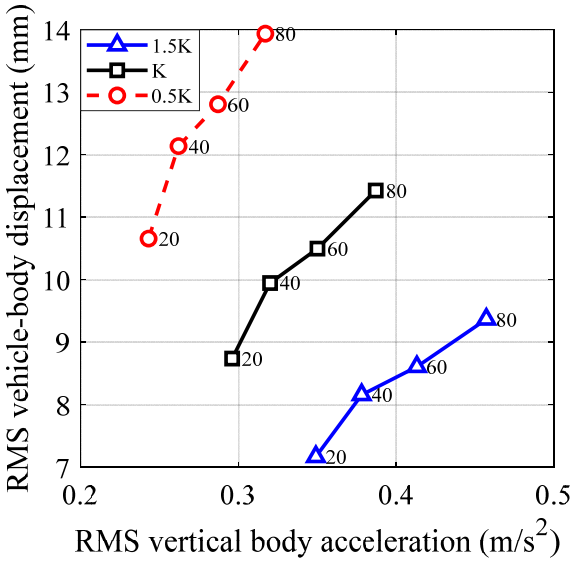


Figure 24. RMS displacement–acceleration trade-off on class D.

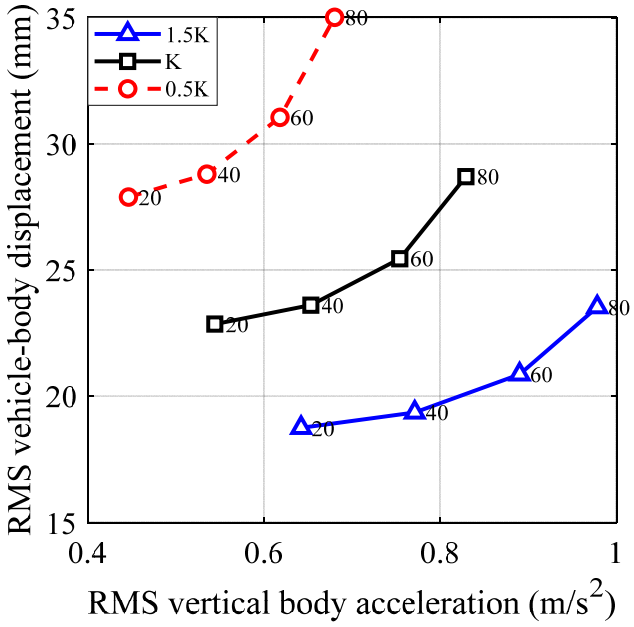


Figure 25. RMS displacement–acceleration trade-off on class E.

The results in Table 3 demonstrate a fundamental trade-off in passive suspension design. Increasing suspension stiffness increases the natural frequency of the sprung-mass system and reduces the low-frequency body displacement. This effect becomes particularly important on rough roads, where large suspension deflections may compromise suspension travel and vehicle-body motion control. However, the increased stiffness also reduces the suspension's isolation capability. It allows a larger portion of the road-induced force to be transmitted to the vehicle body, resulting in higher vertical acceleration. At 80 km/h on the class E road, increasing the stiffness from 0.5 K to 1.5 K reduces the RMS body displacement from 35.01 to 23.53 mm, a reduction of 32.8%, whereas the RMS vertical acceleration increases from 0.680 to 0.978 m/s^2, an increase of 43.8%. Therefore, selecting the maximum stiffness does not represent an optimum solution for riding comfort. Instead, intermediate stiffness should be selected according to the relative importance assigned to body-motion control and passenger comfort.

Table 3. RMS vehicle body displacement and RMS vertical body acceleration when changing suspension stiffness.

Value	***Suspension stiffness***	**Root Mean Square (RMS) Vehicle Body Displacement (mm)**				**Root Mean Square (RMS) Vertical Body Acceleration (m/s^2)**			
Velocity (km/h)		**20**	**40**	**60**	**80**	**20**	**40**	**60**	**80**
class B	1.5 K	0.74	1.01	1.39	1.94	0.077	0.094	0.109	0.119
	K	0.90	1.22	1.71	2.37	0.065	0.080	0.092	0.101
	0.5 K	1.10	1.49	2.09	2.89	0.053	0.066	0.075	0.083
class C	1.5 K	2.79	3.70	4.29	5.03	0.178	0.203	0.224	0.238
	K	3.40	4.51	5.23	6.13	0.151	0.172	0.190	0.202
	0.5 K	4.15	5.50	6.38	7.48	0.124	0.141	0.156	0.166
class D	1.5 K	7.17	8.16	8.61	9.37	0.349	0.378	0.413	0.457
	K	8.74	9.95	10.50	11.43	0.296	0.320	0.350	0.387
	0.5 K	10.66	12.14	12.81	13.94	0.243	0.262	0.287	0.317
class E	1.5 K	18.75	19.36	20.87	23.53	0.642	0.771	0.890	0.978
	K	22.86	23.61	25.45	28.70	0.544	0.653	0.754	0.829
	0.5 K	27.89	28.80	31.05	35.01	0.446	0.535	0.618	0.680

Figure 26 shows that the RMS vehicle-body displacement decreases as the suspension stiffness increases from 0.5 K to 1.5 K for all road classes. The fall is smaller on flat class B roads, but greater on rough ones. On a class E road at 80 km/h, the RMS displacement reduces by 32.8% from 35.01 mm to 23.53 mm. A stiffer suspension reduces the RMS body displacement under intense road excitation, indicating improved control of vehicle-body motion. However, this result alone does not establish an improvement in overall vehicle stability or road holding, which require additional indicators such as dynamic tire loads, suspension travel, and roll/pitch responses.

Meanwhile, the RMS vertical body acceleration described in Figure 27 rises with suspension stiffness. The increase in RMS acceleration at 80 km/h on the class E road from 0.680 m/s^2 to 0.978 m/s^2 is around 43.8%. For the other road classes, the same patterns were observed; however, the difference was less clear on smoother road

surfaces. These results indicate that higher suspension stiffness increases the transmission of road-induced vibrations to the vehicle body, which may adversely affect ride comfort.

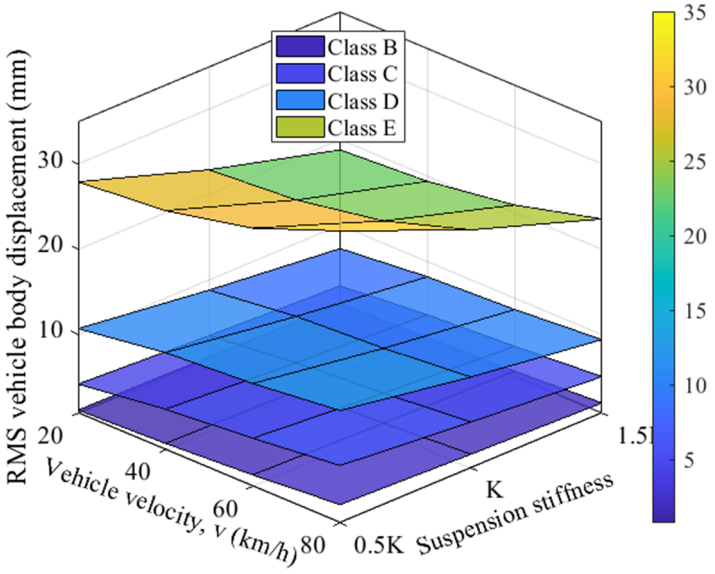


Figure 26. RMS vehicle body displacement.

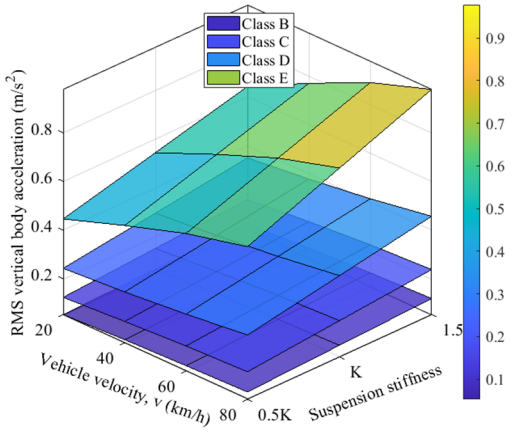


Figure 27. RMS vertical body acceleration.

4. Conclusions

This study developed a seven-degree-of-freedom full-vehicle dynamic model to investigate the vibration characteristics of a passenger vehicle traveling on random road profiles defined by ISO 8608:2016. Based on the simulation results, the following conclusions can be drawn:

Increasing vehicle speed further increases the vibration response, particularly under rough road conditions. At 80 km/h, the RMS vertical body acceleration increases from 0.101 m/s^2 on class B roads to 0.829 m/s^2 on class E roads, while the RMS body displacement increases from 2.37 to 28.70 mm.

Vehicle speed further amplifies the vibration response. On all road classes, increasing speed from 20 to 80 km/h results in higher RMS body displacement and vertical acceleration, with the effect becoming more pronounced as road roughness increases.

Suspension stiffness produces a clear comfort–motion-control trade-off. On the class E road at 80 km/h, increasing stiffness from 0.5 K to 1.5 K reduces RMS body displacement from 35.01 to 23.53 mm, corresponding to a 32.8% reduction. However, RMS vertical acceleration increases from 0.680 to 0.978 m/s^2, corresponding to a 43.8% increase.

The results indicate that increasing suspension stiffness leads to a reduction in RMS body displacement but an increase in RMS vertical acceleration. Therefore, the present results demonstrate a clear trade-off between

body-motion control and vibration isolation rather than identifying a single optimal suspension stiffness. The preferred stiffness level depends on the relative importance of these two vibration-response criteria under different road roughness and vehicle-speed conditions. Conclusions regarding overall vehicle stability, road holding, suspension travel, and dynamic tire-load characteristics are beyond the scope of the present analysis and require additional dynamic-response metrics for further assessment.

The study has drawbacks, including the use of linear spring-damper models, the absence of suspension friction, nonlinear damping, bump-stop effects, tire stiffening, and parameter errors representing suspension and tire properties. Ride-comfort assessment uses time-domain RMS quantities and does not yet include frequency-weighted ISO 2631 measures or vibration dosage values. The experimental validation using car vibration and suspension displacement data is also missing. Future research will therefore focus on three directions: (i) development of nonlinear suspension and tire models with experimentally identified characteristics; (ii) incorporation of frequency-weighted ride-comfort indicators and multi-objective indices involving ride comfort, road holding, roll stability, and pitch control; and (iii) experimental validation of the proposed 7-DOF model under representative ISO 8608 road conditions. These extensions will allow the model to be applied more reliably to practical suspension optimization and vehicle dynamic performance assessment.

Author Contributions: A.N.H.: conceptualization, methodology, software; D.N.Q.: data curation, writing—original draft preparation; D.P.L.X.: visualization, investigation; A.N.H.: supervision; D.N.Q.: software, validation; D.P.L.X.: writing—reviewing and editing. All authors have read and agreed to the published version of the manuscript.

Funding: This research received no external funding.

Institutional Review Board Statement: Not applicable.

Informed Consent Statement: Not applicable.

Data Availability Statement: Not applicable.

Conflicts of Interest: The authors declare no conflicts of interest.

Use of AI and AI-Assisted Technologies: No AI tools were utilized for this paper.

References

1. *ISO 8608*; Mechanical Vibration—Road Surface Profiles—Reporting of Measured Data. International Organization for Standardization: Geneva, Switzerland, 2016.
2. Foo, M.; Tan, A.H. Benchmark vehicle suspension data based on ISO 8608 road profiles. *Control. Eng. Pract.* **2026**, *169*, 106755. https://doi.org/10.1016/j.conengprac.2025.106755.
3. Mieteń, M.; Seńko, J.; Caban, J.; Szcześniak, K.; Walkiewicz, M. Research on Dynamic Loads Acting on a Vehicle Caused by the Road Profile with Different Surfaces. *Appl. Sci.* **2025**, *15*, 13106. https://doi.org/10.3390/app152413106.
4. Wang, Y.; Cao, J.; Huang, W.; Ma, T.; Zhou, Z. Dynamic response analysis of vehicle–pavement-coupled system based on RIOHTrack full-size accelerated loading test. *Constr. Build. Mater.* **2023**, *402*, 132744. https://doi.org/10.1016/j.conbuildmat.2023.132744.
5. Xie, J.; Yan, S.; Feng, C. Dynamic Load Analysis of Vertical, Pitching, and Lateral Tilt Vibrations of Multi-Axle Vehicles. *Appl. Sci.* **2025**, *15*, 9906. https://doi.org/10.3390/app15189906.
6. Zhao, T.; He, J.; Lv, J.; Min, D.; Wei, Y. A Comprehensive Implementation of Road Surface Classification for Vehicle Driving Assistance: Dataset, Models, and Deployment. *IEEE Trans. Intell. Transp. Syst.* **2023**, *24*, 8361–8370. https://doi.org/10.1109/tits.2023.3264588.
7. Douier, K.; Renno, J.; Hussein, M.F.M. Reconstructing Road Roughness Profiles Using ANNs and Dynamic Vehicle Accelerations. *Infrastructures* **2024**, *9*, 198. https://doi.org/10.3390/infrastructures9110198.
8. Xing, J.; Cheng, Z.; Ye, S.; Liu, S.; Lin, J. Road Roughness Recognition: Feature Extraction and Speed-Adaptive Classification Based on Simulation and Real-Vehicle Tests. *Machines* **2025**, *13*, 391. https://doi.org/10.3390/machines13050391.
9. Tan, A.H.; Foo, M.F.L.; Ong, D.S. Road classification using built-in self-scaling method of Bayesian regression. *J. Sound Vib.* **2022**, *516*, 116523. https://doi.org/10.1016/j.jsv.2021.116523.
10. Stan, C.; Oprea, R.A. Vibration Comfort Assessment Methods in Heavy Vehicles: Models, Standards and Numerical Approaches—A State-of-the-Art Review. *Technologies* **2026**, *14*, 98. https://doi.org/10.3390/technologies14020098.
11. *ISO 2631-1*; Mechanical Vibration and Shock—Evaluation of Human Exposure to Whole-Body Vibration—Part 1: General Requirements. International Organization for Standardization: Geneva, Switzerland, 1997.

12. Guastadisegni, G.; De Pinto, S.; Cancelli, D.; Labianca, S.; Gonzalez, A.; Gruber, P.; Sorniotti, A. Ride Analysis Tools for Passenger Cars: Objective and Subjective Evaluation Techniques and Correlation Processes—A Review. *Veh. Syst. Dyn.* **2024**, *62*, 1876–1902. https://doi.org/10.1080/00423114.2023.2259024.
13. Fossati, G.G.; Miguel, L.F.F.; Casas, W.J.P. Multi-objective optimization of the suspension system parameters of a full vehicle model. *Optim. Eng.* **2018**, *20*, 151–177. https://doi.org/10.1007/s11081-018-9403-8.
14. Srikanth, K.; Chowdary, V. Influence of roughness and cross slope induced dynamic loads on flexible pavement responses. *Int. J. Pavement Eng.* **2023**, *24*, 2241101. https://doi.org/10.1080/10298436.2023.2241101.
15. Xu, G.; Zhang, N.; Roser, H.M. Roll and pitch independently tuned interconnected suspension: Modelling and dynamic analysis. *Veh. Syst. Dyn.* **2015**, *53*, 1830–1849. https://doi.org/10.1080/00423114.2015.1103375.
16. Damavandi, A.D.; Masih-Tehrani, M.; Mashadi, B. Configuration development and optimization of hydraulically interconnected suspension for handling and ride enhancement. *Proc. Inst. Mech. Eng. Part D J. Automob. Eng.* **2022**, *236*, 381–394. https://doi.org/10.1177/09544070211018040.
17. Emami, A.; Masih-Tehrani, M.; Amirkhani, A.; Najafi, A. Robust Fuzzy Sliding Mode Controller for the Full Vehicle Semi-Active Suspension System Considering the Impact of Uncertainties. *IET Intell. Transp. Syst.* **2025**, *19*, e70125. https://doi.org/10.1049/itr2.70125.
18. Sun, Q.; Yin, C.; Wang, B. Experimental Validation of Truck Cab Suspension Model and Ride Comfort Improvement under Various Semi-Active Control Strategies. *Processes* **2024**, *12*, 1880. https://doi.org/10.3390/pr12091880.
19. Kim, D.; Jeong, Y. Road-Adaptive Static Output Feedback Control of a Semi-Active Suspension System for Ride Comfort. *Actuators* **2024**, *13*, 394. https://doi.org/10.3390/act13100394.
20. Van Luong, V.; Nguyen, T.Q.; Le, H.Q.; Le, V.A.; Tran, P.H.; Nguyen, X.; Van, T.T. Determination of dynamic loads from the road surface acting on the chassis by experimental methods. *IOP Conf. Ser. Mater. Sci. Eng.* **2020**, *886*, 012008. https://doi.org/10.1088/1757-899x/886/1/012008.
21. Mahmood, A.; Kat, C.J.; Els, P.S. Ride comfort optimization with handling constraints over rough terrain. *J. Terramechanics* **2026**, *122*, 101105. https://doi.org/10.1016/j.jterra.2025.101105.
22. Tehrani, M.M.; Mollajafari, M.; Nazemi, S. GA tuned H_∞ roll acceleration controller based on series active variable geometry suspension on rough roads. *Int. J. Veh. Perform.* **2022**, 8, 166–187. https://doi.org/10.1504/ijvp.2022.10045653.
23. Kimball, J.B.; DeBoer, B.; Bubbar, K. Adaptive control and reinforcement learning for vehicle suspension control: A review. *Annu. Rev. Control.* **2024**, *58*, 100974. https://doi.org/10.1016/j.arcontrol.2024.100974.
24. Wang, G.; Deng, J.; Duan, D. Data-driven H2/H∞ control for full-car active suspension systems via stochastic reinforcement learning algorithm. *Proc. Inst. Mech. Eng. Part C J. Mech. Eng. Sci.* **2025**, *240*, 1303–1321. https://doi.org/10.1177/09544062251406280.